

# Controlling Topological Quantum Transport via Non-Perturbative Light-Matter Interaction in Disordered Systems

Jorge Martínez Romeral,<sup>1,2,\*</sup> Luis M. Canonico,<sup>1,†</sup> Aron W. Cummings,<sup>1</sup> and Stephan Roche<sup>1,3</sup>

<sup>1</sup>*Catalan Institute of Nanoscience and Nanotechnology (ICN2),*

*CSIC and BIST, Campus UAB, Bellaterra, 08193 Barcelona, Spain*

<sup>2</sup>*Department of Physics, Campus UAB, Bellaterra, 08193 Barcelona, Spain*

<sup>3</sup>*ICREA–Institució Catalana de Recerca i Estudis Avançats, 08010 Barcelona, Spain*

(Dated: June 25, 2025)

We report the possibility to induce topological quantum transport in otherwise trivial systems through non-perturbative light-matter interactions, as well as the enhancement of this effect in the presence of disorder. Going beyond prior theoretical approaches, we introduce a computational framework which performs large-scale real-space quantum dynamics simulations, including carrier thermalization and disorder effects, in systems driven out of equilibrium by light or other external interactions. This methodology is illustrated in gapped single-layer and Bernal bilayer graphene but can be implemented in arbitrarily complex systems, including disordered and aperiodic systems, opening novel avenues for the design of multifunctional topological electronic devices that work in far-from-equilibrium regimes.

*Introduction.* Topological systems have been extensively studied since their theoretical inception [1–3] and experimental confirmation [4–11]. Their primary appeal lies in the robustness of quantum transport features, such as quantized Hall conductance, that are topologically protected against disorder effects [12, 13]. However, many of these properties still require strong magnetic fields, low temperatures, or scarce and costly materials, making their industrial implementation challenging [14–16].

In this context, optical excitation has emerged as a promising tool to overcome these limitations by enabling topological properties in more common and simpler materials [17–21]. Theoretical exploration of these phenomena mostly relies on Floquet theory, a widely used framework that has predicted a rich variety of results [18, 21–23]. Nonetheless, experimental realizations remain scarce and often deviate from theoretical predictions, even in relatively simple systems [20, 24–28]. This persistent gap between theory and experiment is largely attributable to the lack of a theoretical framework capable of directly computing bulk observables while fully incorporating realistic conditions – including carrier relaxation, the presence of disorder, or complex light modulation schemes. Current approaches tend to incorporate only a subset of these essential ingredients [17, 29, 30].

Here, we overcome the current limitations by presenting a novel computational framework for quantum transport in systems driven out of equilibrium that includes non-perturbative disorder and carrier relaxation effects in real time. Our methodology allows for a general, non-equilibrium density matrix and utilizes the kernel polynomial method [31, 32], which operates in real space and

enables the simulation of systems with tens of millions of atoms. This facilitates the realistic modeling of disorder effects, as well as amorphous materials [33] or materials with very large unit cells [34]. Carrier relaxation, which drives an excited non-thermal distribution toward a hot thermal distribution, is treated using the methodology previously developed in Ref. [35].

As a demonstration, we first apply our methodology to the topological phase of the Haldane model [2] and to gapped single-layer graphene. We demonstrate that the quantized Hall conductivity of a topological system can be tuned using light. In the case of gapped graphene, which is topologically trivial at equilibrium, we show that light can generate an anomalous Hall conductivity, as reported experimentally [20].

Finally, we examine light-induced Hall conductivity in dual-gated AB-stacked bilayer graphene (BLG). We observe the emergence of an anomalous topological response under realistic conditions, including disorder caused by electron-hole puddles [36, 37] and carrier relaxation times of the order of tens of femtoseconds arising from electron-electron scattering [38]. Our results reveal that electron-electron scattering strongly suppresses the magnitude of the topological response by relaxing the excited electrons toward a hot thermal distribution, while long-range electron-hole puddles have minimal impact. Meanwhile, strong short-range disorder can enhance the response by increasing the number of optically-excited carriers.

*Methodology.* Our methodology consists of two steps. First, we simulate the evolution of the density matrix of a given system under a time-dependent Hamiltonian, and second, we calculate observables such as the electrical conductivity and the excited number of carriers at given points in time.

For the evolution of the density matrix, we follow the methodology presented in Ref. [35], which consists of evolving the ground-state density ma-

\* [jorge.martinez@icn2.cat](mailto:jorge.martinez@icn2.cat)

† [luis.canonico@icn2.cat](mailto:luis.canonico@icn2.cat)

trix under the action of a time-dependent Hamiltonian,  $\hat{H}(t)$ . The system is assumed to initially be in a thermal distribution,  $\hat{\rho}(0) = \hat{\rho}_{\text{thermal}}(0) = \left[1 + \exp\left\{\frac{\hat{H}(0) - \mu(0)}{k_B T(0)}\right\}\right]^{-1}$ , with initial temperature  $T(0)$  and chemical potential  $\mu(0)$ . The system evolves under the time-ordered evolution operator,  $\hat{U}(t_1, t_0) = \hat{\mathcal{T}} \exp\left\{-\frac{i}{\hbar} \int_{t_0}^{t_1} \hat{H}(t') dt'\right\}$ , which for short times can be expressed as  $\hat{U}(t + \Delta t, t) \approx \exp\left\{-i\hat{H}(t)\Delta t/\hbar\right\}$  [39]. Defining the vector  $|\rho(t)\rangle = \hat{U}(t, 0)\hat{\rho}(t=0)|\psi\rangle$ , where  $|\psi\rangle$  is the initial state vector with arbitrary form and  $|\psi(t)\rangle = \hat{U}(t, 0)|\psi\rangle$ , its evolution is given by

$$|\rho(t + \Delta t)\rangle = \left(1 - \frac{\Delta t}{\tau}\right) \hat{U}(t + \Delta t, t) |\rho(t)\rangle + \frac{\Delta t}{\tau} \hat{\rho}_{\text{thermal}}(t + \Delta t) \hat{U}(t + \Delta t, t) |\psi(t)\rangle, \quad (1)$$

where  $\tau$  is the time electrons take to relax to an instantaneous thermal distribution,  $\hat{\rho}_{\text{thermal}}(t + \Delta t)$ . We assume that the main relaxation mechanism is due to electron-electron scattering, and therefore at each time step the chemical potential  $\mu(t)$  and temperature  $T(t)$  are computed to ensure energy and carrier conservation. At the final time,  $t_f$ , the density matrix contains the complete history of the electron occupation during the evolution.

From the density matrix we compute the conductivity tensor  $\sigma_{\alpha\beta}$ , which describes the current along direction  $\alpha$  in response to an applied electric field along  $\beta$ . We derive an expression that allows the introduction of a density matrix of arbitrary form by assuming a linear time-dependent perturbation  $\hat{V} = -f(\tau)\mathbf{r} \cdot \mathbf{E}$ , where  $\mathbf{r}$  is the position operator,  $\mathbf{E}$  is the applied electric field, and  $f(\tau)$  is the time profile of the perturbation, which is set to turn off adiabatically over a timescale  $\tau_\phi$ . The conductivity tensor is then computed as [39, 40],

$$\sigma_{\alpha\beta} = \frac{e^2}{i\hbar\Omega} \lim_{\tau_\phi \rightarrow \infty} \int_0^{\tau_\phi} e^{-\frac{\tau}{\tau_\phi}} \text{Tr}\left\{\hat{\rho}(t_f)\hat{U}^\dagger(\tau, 0)[\hat{v}_\alpha, \hat{r}_\beta]\hat{U}(\tau, 0) + 2\text{Im}\left(\hat{\rho}(t_f)\hat{U}^\dagger(\tau, 0)\hat{v}_\alpha\left[\hat{U}(\tau, 0), \hat{r}_\beta\right]\right)\right\} d\tau, \quad (2)$$

where  $e$  is the electron charge,  $\hbar$  is the reduced Planck constant,  $\Omega$  is the sample area, and  $\hat{v}_\alpha$  is the velocity operator in the  $\alpha$  direction. This formula is evaluated using the non-equilibrium density matrix at the final time, which has undergone the time evolution  $\hat{\rho}(0) \rightarrow \hat{\rho}(t_f)$ , and the Hamiltonian at the final time,  $\hat{H}(t_f)$ . Further details on the derivation of Eq. (2) are provided in the SM [39].

Additionally, we compute the electron occupation of the excited distribution at  $t_f$ , [35, 39],

$$\langle n(E) \rangle = \frac{\text{Tr}\left\{\delta\left(\hat{H}(t_f) - E\right)\hat{\rho}(t_f)\right\}}{\text{Tr}\left\{\delta\left(\hat{H}(t_f) - E\right)\right\}}, \quad (3)$$

where  $\delta(\cdot)$  is the spectral measure operator which projects the occupation onto energy  $E$ .

To evaluate the traces in Eqs. (2) and (3), we use the stochastic trace approximation,  $\text{Tr}\{\hat{A}\} \approx \frac{1}{R} \sum_{i=1}^R \langle \psi_i | \hat{A} | \psi_i \rangle$ , where  $|\psi_i\rangle$  is a complex vector with random phase at each site and  $R$  is the number of random vectors [31, 32, 39]. The error of this approximation scales as  $1/\sqrt{RN}$  where  $N$  is the number of orbitals in the system. We use such random phase states as our initial state in the time evolution of Eq. (1).

To evaluate functions of the Hamiltonian, namely  $\hat{U}(t_1, t_0)$  and  $\delta(\hat{H} - E)$ , instead of diagonalizing  $\hat{H}$  we employ the kernel polynomial method and expand them as a series of Chebyshev polynomials [31, 32, 39]. Together with the stochastic trace approximation, this makes the computation of the out-of-equilibrium conductivity  $\mathcal{O}(N)$ , i.e., the computation time scales linearly with the size of the Hamiltonian, thus permitting simulations involving millions of orbitals. For example, in Figs. 2 and 3 we use 4 and 8 million orbitals respectively.

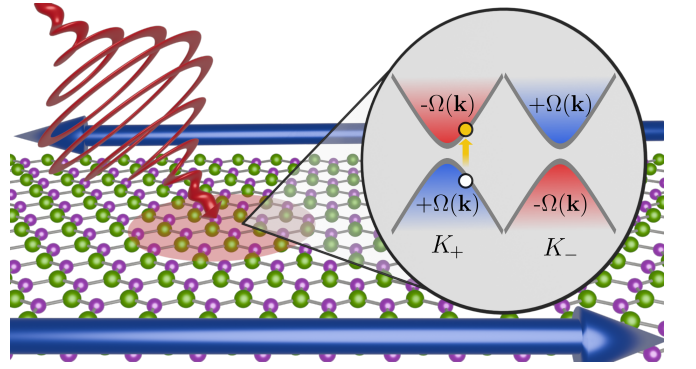


FIG. 1. Schematic of light-induced quantum transport in gapped graphene, via the valley-selective excitation of carriers from the positive-Berry-curvature valence band to the negative-Berry-curvature conduction band.

*Optically excited Haldane model and gapped graphene.* To examine the underlying physical mechanism that drives non-equilibrium topological responses, we introduce the Haldane model [2],

$$\hat{H} = \sum_{\langle ij \rangle} \gamma_{ij} c_i^\dagger c_j \pm m \sum_{i \in A/B} c_i^\dagger c_i + \sum_{\langle\langle ij \rangle\rangle} \gamma_{2,ij} e^{i\phi_{ij}} c_i^\dagger c_j + \text{h.c.} \quad (4)$$

The first term describes nearest-neighbor hopping; we set  $\gamma_{ij} = \gamma = -2.7$  eV, the value in graphene. The second term, positive (negative) on sublattice  $A$  ( $B$ ), breaks inversion symmetry and opens a trivial band gap  $\Delta_m = 2m$ . The third term is a complex second-neighbor hopping that breaks time-reversal symmetry and opens a topological gap  $\Delta_H = 6\sqrt{3}|\gamma_2|$  (here we set  $\phi_{ij} = \pi/2$ ). When both gap-opening terms are nonzero, the total band gap is  $\Delta = |\Delta_m - \Delta_H|$ . When  $\Delta_m > \Delta_H$  the system is a trivial insulator, otherwise it is a Chern insulator [2]. In equilibrium, the Hall conductivity within

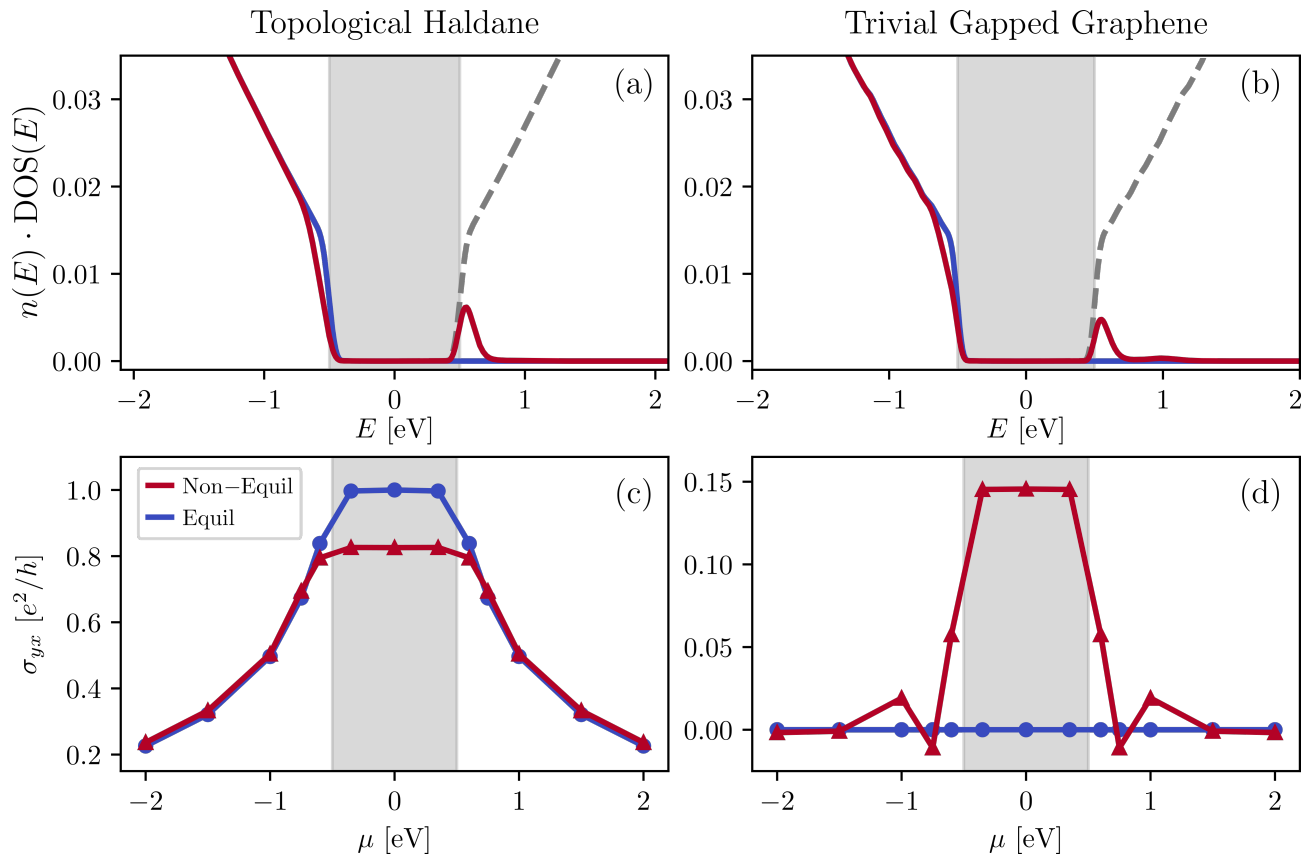


FIG. 2. Top panels: number of carriers multiplied by the density of states, for  $\mu = 0$  eV, in equilibrium/non-equilibrium in blue/red, respectively, jointly with the density of states in grey dashed lines, for the topological Haldane and trivial gapped graphene in the left and right panels. Bottom panels: Hall equilibrium/non-equilibrium conductivity in blue/red, respectively, for different chemical potentials for the topological Haldane and trivial gapped graphene in the left and right panels. The shaded areas in all the plots represent the gap.

the band gap is given by  $\sigma_{yx} = \mathcal{C} \cdot e^2/h$ , where  $\mathcal{C} = 0$  (1) is the Chern number in the trivial (topological) phase [2].

We consider the topological phase by setting  $m = 0$  and  $\gamma_2 = 1/(6\sqrt{3})$  eV, and the trivial phase by setting  $m = 0.5$  eV and  $\gamma_2 = 0$ . Both phases have the same DOS with a band gap of 1 eV, as indicated by the dashed gray lines in Figs. 2(a,b). Despite their identical DOS, the difference between these two systems is revealed in their equilibrium Hall conductivity, calculated using Eq. (2) at  $t = 0$  and shown as the blue lines in Figs. 2(c,d). As mentioned above, the topological phase exhibits  $\sigma_{yx} = e^2/h$  within the gap, while for the trivial phase  $\sigma_{yx} = 0$ .

This behavior can be understood by considering the Chern number, which arises from the sum of the Berry curvature ( $\Omega$ ) in both valleys, shown schematically in Fig. 1. Depending on the Berry curvature polarization in each valley, the sum will result in  $\mathcal{C} = 0$  or 1. In the topological case,  $\Omega > 0$  in both valleys, summing up to a non-zero contribution. Meanwhile, in the trivial phase,  $\Omega$  has opposite sign in each valley, perfectly canceling and leading to  $\mathcal{C} = 0$  [2]. In addition, the Berry curvature has opposite sign in the valence and conduction bands, resulting in a vanishing Hall conductivity outside of the gap.

To drive the system out of equilibrium, we apply an optical pulse with vector potential  $\mathbf{A}(t) = A_0 P(t) (\cos(\omega_p t) \hat{x} + \eta \sin(\omega_p t) \hat{y})$ , where  $A_0$  is the amplitude,  $P(t)$  is the pulse envelope,  $\hbar\omega_p$  is the photon energy, and  $\eta = \pm 1$  corresponds to right/left circular polarization [41]. The envelope function is set as  $P(t) = \text{sech}[(t - 2T_p)/(bT_p)]$ . Here we consider a short pulse of just a few optical periods by letting  $T_p = 2\pi/\omega_p$  and  $b \approx 0.5673$ , such that the full width at half maximum of  $P^2(t)$  is  $T_p$  [42]. Using the Peierls substitution, the neighbor hoppings in the Hamiltonian become time dependent,

$$\gamma_{ij}(t) = \gamma \exp\left(i \frac{2\pi}{\Phi_0} \int_{\mathbf{r}_i}^{\mathbf{r}_j} d\mathbf{r} \cdot \mathbf{A}(t)\right), \quad (5)$$

where  $\mathbf{r}_i$  is the position of site  $i$  and  $\Phi_0 = h/e$  is the magnetic flux quantum. In the following, we set  $A_0 = \Gamma\Phi_0/2a$ , where  $\Gamma$  is a dimensionless free parameter that controls the strength of the pulse and  $a = 0.246$  nm is the graphene lattice constant.

In what follows, we consider irradiation times up to  $4T_p$ , covering the full range of the optical pulse. During this period, we evolve the system using Eq. (1), and

once the pulse ends we calculate the conductivity and the number of excited carriers of the resulting out-of-equilibrium system using Eqs. (2) and (3). We consider a circularly-polarized optical pulse with a photon energy of  $\hbar\omega_p = 1$  eV, corresponding to the topological or trivial band gap, and a pulse strength of  $\Gamma = 2.5 \cdot 10^{-2}$ . At this photon energy,  $4T_p \approx 16$  fs, shorter than the typical electron-electron thermalization time of graphene, so for these simulations we let  $\tau \rightarrow \infty$ .

The solid lines in Fig. 2(a) show the carrier occupation before (blue) and after (red) optical excitation, indicating a transfer of carriers from  $-\hbar\omega_p/2$  to  $+\hbar\omega_p/2$  for both the topological and the trivial phases. The higher number of transferred carriers in the topological case reflects the fact that both valleys are excited, while in the trivial case only one valley is excited (see Fig. 1). These changes in carrier occupation manifest in the Hall conductivity,  $\sigma_{yx}$ , which from this point onward is defined as the difference between left and right circular polarization,  $\sigma_{yx} = (\sigma_{yx}^{\circlearrowleft} - \sigma_{yx}^{\circlearrowright})/2$ , following the convention commonly used in experiments [20]. This behavior is illustrated in Fig. 2(b).

In the topological phase at  $\mu = 0$ , circularly polarized light excites all available carriers in both valleys, transferring electrons from regions with positive Berry curvature to regions with negative Berry curvature [43]. As a result, the total Hall conductivity becomes smaller than in the equilibrium case. In the trivial phase, circularly polarized light excites electrons from only one valley [43], which now contributes with the opposite sign of Berry curvature. As the contributions from the two valleys no longer cancel, this leads to a non-zero Hall conductivity. In both cases, the resulting non-equilibrium conductivity can be tuned by adjusting the pulse duration or intensity, which controls the number of excited carriers and, consequently, the total integral of the Berry curvature over the occupied states.

*Disorder enhanced quantum anomalous Hall conductivity in BLG.* We now apply the method to Bernal BLG, whose Hamiltonian consists of two copies of the first term of Eq. (4), plus two additional terms: a vertical hopping term  $\gamma_3 = 0.4$  eV between A atoms in the bottom layer and B atoms in the top layer, and a mass term  $U$  that breaks the symmetry between the layers and consequently opens a gap [44]. This latter term can be induced experimentally through doping or the use of external gates. In the following we set  $U = 0.23$  eV, which opens a gap of  $\Delta = 0.2$  eV, a value shown to be experimentally realizable [45]. We consider the same optical pulse parameters as before while setting  $\hbar\omega_p \approx \Delta$ , which corresponds to a fluence of  $F = 0.04$  mJ/cm<sup>2</sup> [39]. In this case  $4T_p \approx 83$  fs, and thus we set the electron-electron relaxation time  $\tau = 25$  fs, which is consistent with experimental estimates for graphene [46] and for matching simulations to measurements of saturable absorption [35].

The behavior observed in gapped BLG is analogous to that of gapped single-layer graphene, where the Berry curvature of the valence bands from both valleys cancels

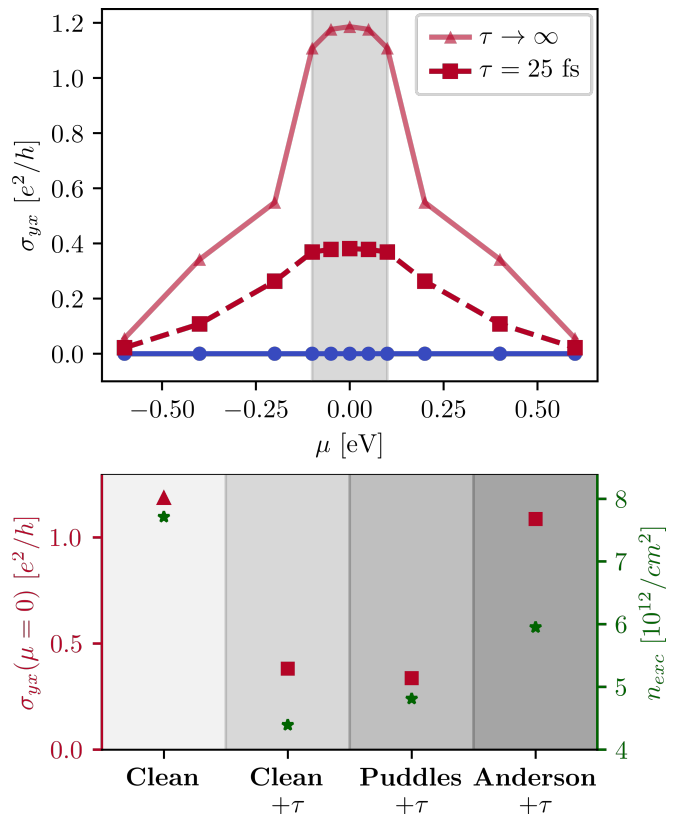


FIG. 3. Top panel: Hall conductivity of BLG as a function of the chemical potential in equilibrium (blue line) and after optical excitation (red lines), for carrier thermalization times  $\tau \rightarrow \infty$  and  $\tau = 25$  fs. Bottom panel: The left axis indicates the Hall conductivity at  $\mu = 0$  for the clean case and for different disorder conditions described in the main text. The leftmost result shows the case for  $\tau \rightarrow \infty$  and all other cases are for  $\tau = 25$  fs. The right axis shows the corresponding number of excited carriers for each phase indicated in the horizontal axis.

out, resulting in zero Hall conductivity in equilibrium – see the blue line in the top panel of Fig. 3. In contrast, driving the system out of equilibrium with circularly polarized light leads to an imbalance in valley occupation, giving rise to an anomalous Hall conductivity, as shown by the red lines. Introducing a finite carrier thermalization time significantly suppresses the response. This reduction occurs because the carrier relaxation tends to drive the excited carrier population toward a hot electron distribution that mainly occupies the valence band.

Next, we consider the presence of different types of disorder: electron-hole puddles and Anderson-like disorder. Electron-hole puddles, arising from trapped charges in the substrate, are a type of long-range disorder that is ubiquitous in graphene devices [47, 48] and may be modeled as a series of Gaussian electrostatic impurities added to the onsite energy of the graphene layer [36, 37],

$$V(\mathbf{r}_i) = \sum_{j=1}^{N_{eh}} W_j \exp \left[ -\frac{1}{2} \left( \frac{\mathbf{r}_i - \mathbf{R}_j}{\xi} \right)^2 \right],$$

where  $\mathbf{r}_i$  is the position of each carbon atom,  $\mathbf{R}_j$  is the center of each

puddle,  $N_{\text{eh}}$  is the number of puddles,  $\xi$  is the puddle width, and  $W_j$  chosen randomly in the interval  $[-W, W]$ . Here we set  $W = 35$  meV and  $\xi = 3.5$  nm with a concentration  $n = N_{\text{eh}}/N = 0.0004$  [36, 49]. We also consider Anderson disorder as a model of short-range disorder that may be present in graphene [50], which corresponds to the limit  $\xi \rightarrow 0$  and  $n = N_{\text{eh}}/N = 1$ . In this case we choose  $W = 1.2$  eV, which yields a similar density of states as the electron-hole puddles [39].

The anomalous Hall conductivity at  $\mu = 0$  for both types of disorder is shown in the bottom panel of Fig. 3, along with the results for the clean case with and without thermalization. In the case of electron-hole puddles, the conductivity remains similar to the clean case, as these long-range inhomogeneities primarily induce weak intravalley scattering. In contrast, the presence of Anderson disorder leads to an enhancement in conductivity. This can be attributed to a greater number of excited carriers enabled by the disorder, as indicated by the green markers in the bottom panel of Fig. 3. A similar enhancement of absorption efficiency in single-layer graphene has previously been reported, which was attributed to additional optical absorption pathways being opened by the short-range disorder [35, 39]. This behavior may initially appear counterintuitive; although Anderson disorder enables a higher density of excited carriers, it also introduces stronger intervalley scattering compared to electron-hole puddles, which will decrease the valley polarization and therefore the Hall conductivity. However, for this Anderson disorder strength, the intervalley scattering occurs on the  $\sim 100$ -fs scale and thus leads to a weaker reduction in conductivity compared to the electron-electron scattering.

*Summary and conclusions.* This work introduces

a novel computational framework for simulating non-equilibrium transport phenomena in quantum materials under optical excitation, while including carrier thermalization and disorder. Using this methodology, we demonstrate how the topological properties of two-dimensional materials can be dynamically controlled, giving rise to Hall conductivities even in systems that are topologically trivial at equilibrium. Our results reveal that these emergent anomalous conductivities are highly sensitive to the thermalization of photoexcited carriers, leading to a suppression of the response. Conversely, they can be significantly enhanced in the presence of disorder.

Although illustrated here for optical excitation of two-dimensional quantum systems, the framework is general and can be extended to models of arbitrary complexity, including moiré or aperiodic materials, as well as arbitrary external excitations including strain, heat, etc. This versatility opens new avenues for the design and engineering of multifunctional topological electronic and spintronic devices.

#### ACKNOWLEDGMENTS

We acknowledge funding from MCIN/AEI/10.13039/501100011033 and European Union "NextGenerationEU/PRTR" under grant PCI2021-122035-2A-2a. ICN2 is funded by the CERCA Programme Generalitat de Catalunya and supported by the Severo Ochoa Centres of Excellence programme, Grant CEX2021-001214-S, funded by MCIN/AEI/10.13039.501100011033. This work is also supported by MICIN with European funds-NextGenerationEU (PRTR-C17.I1) and by and 2021 SGR 00997, funded by Generalitat de Catalunya.

- 
- [1] D. J. Thouless, M. Kohmoto, M. P. Nightingale, and M. den Nijs, Quantized Hall conductance in a two-dimensional periodic potential, *Physical Review Letters* **49**, 405–408 (1982).
  - [2] F. D. M. Haldane, Model for a quantum Hall effect without Landau levels: Condensed-matter realization of the "parity anomaly", *Physical Review Letters* **61**, 2015 (1988).
  - [3] C. L. Kane and E. J. Mele, Z<sub>2</sub> topological order and the quantum spin Hall effect, *Physical Review Letters* **95**, 146802 (2005).
  - [4] K. v. Klitzing, G. Dorda, and M. Pepper, New method for high-accuracy determination of the fine-structure constant based on quantized Hall resistance, *Physical Review Letters* **45**, 494–497 (1980).
  - [5] M. König, S. Wiedmann, C. Brüne, A. Roth, H. Buhmann, L. W. Molenkamp, X.-L. Qi, and S.-C. Zhang, Quantum spin Hall insulator state in HgTe quantum wells, *Science* **318**, 766 (2007).
  - [6] D. Hsieh, D. Qian, L. Wray, Y. Xia, Y. S. Hor, R. J. Cava, and M. Z. Hasan, A topological Dirac insulator in a quantum spin Hall phase, *Nature* **452**, 970–974 (2008).
  - [7] C.-Z. Chang, J. Zhang, X. Feng, J. Shen, Z. Zhang, M. Guo, K. Li, Y. Ou, P. Wei, L.-L. Wang, Z.-Q. Ji, Y. Feng, S. Ji, X. Chen, J. Jia, X. Dai, Z. Fang, S.-C. Zhang, K. He, and Y. Wang, Experimental observation of the quantum anomalous Hall effect in a magnetic topological insulator, *Science* **340**, 167–170 (2013).
  - [8] M. Z. Hasan and C. L. Kane, Colloquium: Topological insulators, *Reviews of Modern Physics* **82**, 3045 (2010).
  - [9] X.-L. Qi and S.-C. Zhang, Topological insulators and superconductors, *Reviews of Modern Physics* **83**, 1057–1110 (2011).
  - [10] N. Armitage, E. Mele, and A. Vishwanath, Weyl and Dirac semimetals in three-dimensional solids, *Reviews of Modern Physics* **90**, 015001 (2018).
  - [11] B. Weber, M. S. Fuhrer, X.-L. Sheng, S. A. Yang, R. Thomale, S. Shamim, L. W. Molenkamp, D. Cobden, D. Pesin, H. J. W. Zandvliet, P. Bampoulis, R. Claessen, F. R. Menges, J. Gooth, C. Felser, C. Shekhar, A. Tadich, M. Zhao, M. T. Edmonds, and J. Jia, 2024 roadmap on 2d topological insulators, *Journal of Physics Materials* **7**, 022501–022501 (2024).
  - [12] J. H. García, L. Covaci, and T. G. Rappoport, Real-

- space calculation of the conductivity tensor for disordered topological matter, *Physical Review Letters* **114**, 116602 (2015).
- [13] J. M. Romeral, A. W. Cummings, and S. Roche, Scaling of the integrated quantum metric in disordered topological phases, *Physical Review B* **111**, 134201 (2025).
- [14] A. Bansil, H. Lin, and T. Das, Colloquium: Topological band theory, *Reviews of Modern Physics* **88**, 021004 (2016).
- [15] Y. Tokura, K. Yasuda, and A. Tsukazaki, Magnetic topological insulators, *Nature Reviews Physics* **1**, 126–143 (2019).
- [16] G. B. Haxel, J. B. Hedrick, and G. J. Orris, *Rare earth elements: Critical resources for high technology* (2005).
- [17] T. Oka and H. Aoki, Photovoltaic Hall effect in graphene, *Physical Review B* **79**, 081406 (2009).
- [18] G. Usaj, P. M. Perez-Piskunow, L. E. F. Foa Torres, and C. A. Balseiro, Irradiated graphene as a tunable Floquet topological insulator, *Physical Review B* **90**, 115423 (2014).
- [19] P. M. Perez-Piskunow, G. Usaj, C. A. Balseiro, and L. E. F. F. Torres, Floquet chiral edge states in graphene, *Physical Review B* **89**, 121401 (2014).
- [20] J. W. McIver, B. Schulte, F.-U. Stein, T. Matsuyama, G. Jotzu, G. Meier, and A. Cavalleri, Light-induced anomalous Hall effect in graphene, *Nature Physics* **16**, 38–41 (2019).
- [21] C. Bao, P. Tang, D. Sun, and S. Zhou, Light-induced emergent phenomena in 2D materials and topological materials, *Nature Reviews Physics* **4**, 33–48 (2021).
- [22] N. H. Lindner, G. Refael, and V. Galitski, Floquet topological insulator in semiconductor quantum wells, *Nature Physics* **7**, 490–495 (2011).
- [23] M. S. Rudner and N. H. Lindner, Band structure engineering and non-equilibrium dynamics in Floquet topological insulators, *Nature Reviews Physics* **2**, 229–244 (2020).
- [24] Y. H. Wang, H. Steinberg, P. Jarillo-Herrero, and N. Gedik, Observation of Floquet-Bloch states on the surface of a topological insulator, *Science* **342**, 453–457 (2013).
- [25] A. Tomadin, S. M. Hornett, H. I. Wang, E. M. Alexeev, A. Candini, C. Coletti, D. Turchinovich, M. Kläui, M. Bonn, F. H. L. Koppens, E. Hendry, M. Polini, and K.-J. Tielrooij, The ultrafast dynamics and conductivity of photoexcited graphene at different fermi energies, *Science Advances* **4**, 5313 (2018).
- [26] J. Yin, C. Tan, D. Barcons-Ruiz, I. Torre, K. Watanabe, T. Taniguchi, J. C. W. Song, J. Hone, and F. H. L. Koppens, Tunable and giant valley-selective Hall effect in gapped bilayer graphene, *Science* **375**, 1398–1402 (2022).
- [27] M. Merboldt, M. Schüler, D. Schmitt, J. P. Bange, W. Bennecke, K. Gadge, K. Pierz, H. W. Schumacher, D. Momeni, D. Steil, S. R. Manmana, M. A. Sentef, M. Reutz, and S. Mathias, Observation of Floquet states in graphene, *Nature Physics* **21**, 1745 (2025).
- [28] D. Choi, M. Mogi, U. De Giovannini, D. Azouy, B. Lv, Y. Su, H. Hübener, A. Rubio, and N. Gedik, Observation of Floquet–Bloch states in monolayer graphene, *Nature Physics* , 02888 (2025).
- [29] A. Tomadin, D. Brida, G. Cerullo, A. C. Ferrari, and M. Polini, Nonequilibrium dynamics of photoexcited electrons in graphene: Collinear scattering, auger processes, and the impact of screening, *Physical Review B* **88**, 035430 (2013).
- [30] N. Tancogne-Dejean, M. J. T. Oliveira, X. Andrade, H. Appel, C. H. Borca, G. Le Breton, F. Buchholz, A. Castro, S. Corni, A. A. Correa, U. De Giovannini, A. Delgado, F. G. Eich, J. Flick, G. Gil, A. Gomez, N. Helbig, H. Hübener, R. Jestädt, and J. Jornet-Somoza, Octopus, a computational framework for exploring light-driven phenomena and quantum dynamics in extended and finite systems, *The Journal of Chemical Physics* **152**, 124119 (2020).
- [31] A. Weiße, G. Wellein, A. Alvermann, and H. Fehske, The kernel polynomial method, *Reviews of Modern Physics* **78**, 275–306 (2006).
- [32] Z. Fan, J. H. Garcia, A. W. Cummings, J. E. Barrios-Vargas, M. Panhans, A. Harju, F. Ortman, and S. Roche, Linear scaling quantum transport methodologies, *Physics Reports* **903**, 1–69 (2020).
- [33] T. Galvani, A. K. Hamze, L. Caputo, O. Kaya, S. M.-M. Dubois, L. Colombo, V.-H. Nguyen, Y. Shin, H.-J. Shin, J.-C. Charlier, and S. Roche, Exploring dielectric properties in atomistic models of amorphous boron nitride, *Journal of Physics Materials* **7**, 035003–035003 (2024).
- [34] P. A. Guerrero, V.-H. Nguyen, J. M. Romeral, A. W. Cummings, J.-H. Garcia, J.-C. Charlier, and S. Roche, Disorder-induced delocalization in magic-angle twisted bilayer graphene, *Physical Review Letters* **134**, 126301 (2025).
- [35] L. M. Canonico, S. Roche, and A. W. Cummings, Real-time out-of-equilibrium quantum dynamics in disordered materials, [arXiv:2407.16544](https://arxiv.org/abs/2407.16544).
- [36] S. Adam, S. Jung, N. N. Klimov, N. B. Zhitenev, J. A. Stroscio, and M. D. Stiles, Mechanism for puddle formation in graphene, *Physical Review B* **84**, 235421 (2011).
- [37] D. V. Tuan, S. Adam, and S. Roche, Spin dynamics in bilayer graphene: Role of electron-hole puddles and dyakonov-perel mechanism, *Physical Review B* **94**, 041405 (2016).
- [38] D. Brida, A. Tomadin, C. Manzoni, Y. J. Kim, A. Lombardo, S. Milana, R. R. Nair, K. S. Novoselov, A. C. Ferrari, G. Cerullo, and M. Polini, Ultrafast collinear scattering and carrier multiplication in graphene, *Nature Communications* **4**, 1987 (2013).
- [39] See Supplemental Material at [URL will be inserted by publisher] for a detailed description of the kernel polynomial method and a derivation of the formalism used to obtain the out-of-equilibrium Kubo formula for the electrical conductivity. Additionally, we show the density of states of disordered Bernal bilayer graphene and the formula to compute the fluency of the irradiated light.
- [40] C. Aversa and J. E. Sipe, Nonlinear optical susceptibilities of semiconductors: Results with a length-gauge analysis, *Physical Review B* **52**, 14636–14645 (1995).
- [41] H. L. Calvo, H. M. Pastawski, S. Roche, and L. E. F. Foa Torres, Tuning laser-induced band gaps in graphene, *Applied Physics Letters* **98**, 232103 (2011).
- [42] U. Keller, *Ultrafast Lasers* (Springer International Publishing, 2021).
- [43] K. Ghalamkari, Y. Tatsumi, and R. Saito, Perfect circular dichroism in the haldane model, *Journal of the Physical Society of Japan* **87**, 063708 (2018).
- [44] E. McCann and M. Koshino, The electronic properties of bilayer graphene, *Reports on Progress in Physics* **76**, 056503 (2013).
- [45] Y. Zhang, T.-T. Tang, C. Girit, Z. Hao, M. C. Martin,

- A. Zettl, M. F. Crommie, Y. R. Shen, and F. Wang, Direct observation of a widely tunable bandgap in bilayer graphene, *Nature* **459**, 820–823 (2009).
- [46] M. Massicotte, G. Soavi, A. Principi, and K.-J. Tielrooij, Hot carriers in graphene – fundamentals and applications, *Nanoscale* **13**, 8376–8411 (2021).
- [47] J. Martin, N. Akerman, G. Ulbricht, T. Lohmann, J. H. Smet, K. von Klitzing, and A. Yacoby, Observation of electron–hole puddles in graphene using a scanning single-electron transistor, *Nature Physics* **4**, 144–148 (2007).
- [48] A. Deshpande, W. Bao, F. Miao, C. N. Lau, and B. J. LeRoy, Spatially resolved spectroscopy of monolayer graphene on SiO<sub>2</sub>, *Physical Review B* **79**, 205411 (2009).
- [49] G. M. Rutter, S. Jung, N. N. Klimov, D. B. Newell, N. B. Zhitenev, and J. A. Stroscio, Microscopic polarization in bilayer graphene, *Nature Physics* **7**, 649–655 (2011).
- [50] P. W. Anderson, Absence of diffusion in certain random lattices, *Physical Review* **109**, 1492–1505 (1958).